Self-assembly of complex structures in a two-dimensional system with competing interaction forces

Y. H. Liu,[1] L. Y. Chew,[1] and M. Y. Yu[2,3]

[1]*Division of Physics and Applied Physics, School of Physical and Mathematical Sciences, Nanyang Technological University, Singapore 637371*

[2]*Institute for Fusion Theory and Simulation, Department of Physics, Zhejiang University, Hangzhou 310027, China*

[3]*Theoretische Physik I, Ruhr-Universität Bochum, D-44780 Bochum, Germany*

(Received 10 August 2008; published 18 December 2008)

Self-assembly of minimum-energy configurations of a two-dimensional system consisting of charged particles confined in a quadratic trap and interacting through competing repulsive and attractive interparticle forces is studied by means of molecular dynamics simulation. It is shown that complex configurations, including concentric shells separated by bandlike voids, connected shells with multiple regularly arranged voids, as well as small clusters of particles organized into crystal- or liquidlike structures, can exist. With increase of the particle number, a larger variety of structural patterns becomes possible. The results here are useful for a better understanding of pattern formation in two-dimensional systems, as well as in the design of specific structures for technological applications.

DOI: 10.1103/PhysRevE.78.066405 PACS number(s): 52.27.Lw, 61.50.Ah, 36.40.Wa, 61.43.Bn

I. INTRODUCTION

Self-assembly is the formation of specific structures or patterns from simple constituents without external influence [1–3]. Studies of self-assembly in two- and three-dimensional systems with competing attractive and repulsive interaction forces among the constituent particles have uncovered a wide variety of interesting domain patterns and structures [4–10]. For example, in colloidal systems, a stable fluidic phase appears after the addition of a polymer because of the competition between the polymer induced effective attractive force between the clusters of charged colloids and the intrinsic intercolloidal repulsive force [4,5]. In magnetic materials, the competition between the short-ranged exchange and long-range dipole interactions can lead to domain structures with alternating spin orientation patterns [6]. Self-assembly into rings by charged superparamagnetic spheres can occur on a flat dielectric surface under the influence of a rotating magnetic field. Here the self-assembly is mediated by electrostatic forces: attraction between the negatively charged regions of the dielectric surface and the positively charged spheres, and repulsion between the like-charged spheres [7]. Interesting clumpy, filamentary, and crystalline phases can appear in two-dimensional (2D) periodic systems of charged particles interacting through a competition of short-ranged attractive and long-ranged repulsive forces at different particle densities, as discovered by Reichhardt and co-workers [8,9] through molecular dynamics (MD) simulations. They also found that stripe or labyrinth phases can emerge in a driven system. Nelissen *et al.* [10] investigated a 2D system of trapped charged particles experiencing competing pure interparticle Coulomb repulsive forces and short-ranged attractive forces using Monte Carlo simulation. They discovered that depending on the relative importance of the attractive potential, the particles can organize themselves into bubbles, stripes, or ringlike configurations. Their results also indicate that the overall system configuration depends on the total number of particles in the system.

The total number of particles in a system of interacting particles is an important factor for the occurrence of specific complex structures. In particular, it is of interest to see if new complex structures will appear when the particle number is larger than 100, which is used in Nelissen *et al.*'s studies [10]. In addition, in many systems of current interest, such as the dusty plasma [11–14] and colloidal fluids [15,16], the interparticle repulsive potential is in the form of a screened Coulomb potential. Theoretical studies have also demonstrated that in dusty plasmas the interaction between the charged dust particles can be more complicated when the effects of ion-neutral collisions and ion absorption on the particles are taken into account. At short and moderate separation distances, the electrostatic interaction can be modeled by a screened Coulomb potential, and at larger distances the potential exhibits a Coulomb-like decay [17,18]. In highly collisional plasmas, due to thermionic electron emission from the dust particles and dust shadowing effects, a well can appear in the interparticle potential, leading to an attractive force between the particles [18,19]. In some colloidal systems, the interparticle attractive potential can also be controlled and tailored [20–22]. For example, in a solution of globular proteins the range of the attractive interaction can be controlled by modifying the ionic strength [20]. In a mixture of colloidal particles and nonadsorbing polymer, the length of the polymer determines the attractive interaction range, and the amount of polymer in the solution determines the interaction strength [21,22]. Recently, Liu *et al.* [23,24] have investigated a larger system consisting of multispecies charged particles of different mass and charge interacting through competing long-ranged (short-ranged) repulsive and short-ranged (long-ranged) attractive potential in a 2D quadratic trap. The attractive potential is introduced to simulate the effects of the background plasma as well as the close-neighbor dust particles, and the strength of the attractive interparticle force is very weak compared to the repulsive force, hence the main features of the self-organized structures cannot be affected very much by the attractive interpar-

ticle potential. The particles are also subjected to a radial drag force that is directed towards the system boundary. It is found that in the multispecies particle system shells separated by bandlike voids can occur. In a single-species particle system, only a single shell with a central void can be formed in the presence of a suitable ion drag force [23,24]. Experimental and theoretical studies have also shown that the ion drag force is necessary for the formation of voids in dusty discharges [25–28]. On the other hand, voids can also appear in colloidal polymer dispersions without any drag force [29] if there is an attractive force between the colloidal particles [21,22,29]. These results have motivated us to extend the repulsive Coulomb interparticle force used by Nelissen *et al.* to a screened Coulomb force and to vary the range and strength of the attractive interparticle force and investigate their effects on the steady-state configurations of the system. In order to uncover new steady-state configurations in such a system, we shall consider here an attractive force that is comparable to the repulsive force. We shall also consider the effect of a larger number of particles on the system minimum-energy configurations. In order that the results here be valid for colloidal as well as charged-dust systems, the ion drag force [23–28], which is unique for dusty discharge plasmas, is not included. Our study should be useful for the understanding of pattern formation in 2D confined systems with single as well as multiple species of particles, or other systems with competing interaction forces. They are also useful in the design of small structures used in nanotechnological applications [30].

The paper is organized as follows. In Sec. II, we present and discuss our 2D model system, focusing on a single-species system of charged particles confined in a quadratic trap and interacting through competing attractive and repulsive potentials. The details of the MD simulation process are also given. In Sec. III, we investigate the different minimum-energy configurations of our system with respect to the strength of the attractive and repulsive forces. A conclusion is given in Sec. IV.

II. MODEL SYSTEM

We assume that the interparticle interaction is governed by a pure or screened Coulomb repulsive potential [31–37] and a short-ranged attractive potential as given in Refs. [8–10,23]. The particles are confined by a 2D quadratic trap centered at the origin [38–43], and are constrained to move on a horizontal (x,y) plane. The dimensionless Hamiltonian of the system is $H=K+U$, where K is the kinetic energy, and

$$U=\sum_{i=1}^{N} U_i+\sum_{i<j}^{N} U_{ij} \tag{1}$$

is the potential energy, where N is the total number of particles, $U_i=m\mathbf{r}_i^2$ is the confinement potential energy of the particle i $(=1,\ldots,N)$ located at position $\mathbf{r}_i$ in the quadratic trap, and $U_{ij}=q^2e^{-\alpha r_{ij}}/r_{ij}-Be^{-\beta r_{ij}}$ is the interparticle potential energy between the particles i and j separated by a distance $r_{ij}=|\mathbf{r}_i-\mathbf{r}_j|$. In Eq. (1), the length and energy are normalized by $r_0=(2Q^2/M\varepsilon\omega_0^2)^{1/3}$ and $E_0=M\omega_0^2r_0^2/2$, respectively, where M and Q are the reference mass and charge, ω_0 is the trapping frequency, and ε is the dielectric constant of the medium. In the expressions U_i and U_{ij}, m and q are the particle mass and charge normalized by M and Q, respectively. In U_{ij}, the first and second terms are the repulsive and attractive interparticle potential energies, respectively, and the parameters α^{-1}, β^{-1}, and B characterize the repulsive-potential screening length, the attractive-potential screening length, and the strength of the attractive potential, respectively. In the minimum-energy state, we expect $H\to U$.

Molecular dynamics simulation is used to follow the evolution of the particles. The equation of motion for particle i $(=1,\ldots,N)$ is

$$m\frac{d^2\mathbf{r}_i}{dt^2}=-\nabla\left(U_i+\sum_{j\neq i}^{N}U_{ij}\right)-m\nu\frac{d\mathbf{r}_i}{dt}, \tag{2}$$

where $\nabla=\mathbf{e}_x\partial_x+\mathbf{e}_y\partial_y$, $\mathbf{e}_x$ and $\mathbf{e}_y$ are the unit vectors in the x and y directions, respectively, t is time (normalized by $\sqrt{2}\omega_0^{-1}$), and ν is the frictional coefficient due to collisions with the neutral particles in the medium. In the simulation, a Nosé-Hoover thermostat [44] is used to control the system temperature, and the frictional coefficient ν depends on the instantaneous thermal kinetic energy of the system. The temperature is determined from $T=\Sigma_{i=1}^{N}(m\mathbf{v}_i^2)/2N$ (in unit of E_0), where $\mathbf{v}_i=d\mathbf{r}_i/dt$ is the velocity of particle i. A cutoff radius of $r_c=30$ is used in calculating the interparticle potential energy. We use the Verlet integrator [45] to solve Eq. (2). The integration time step is $0.003\omega_0^{-1}$. We start each run from an initial random phase-space particle distribution at a high temperature $T=0.05\to1.0$. The system is then slowly annealed at a rate $\Delta T=2.5\times10^{-9}$/step until a minimum-energy state is reached at a temperature $T\lesssim\mathcal{O}(10^{-6})$. The annealing rate is kept low in order to prevent the system from being quenched into possible intermediate metastable states. The accuracy of the simulation has been verified by reproducing the ground-state configurations of the clusters found in Ref. [10] which used the Monte Carlo method. We also ran the same systems with different random initial spatial and velocity distributions and found the same final steady-state configurations, which further verified our program. We investigate the minimum-energy configurations for different combinations of the repulsive-potential screening length α^{-1}, attractive-potential screening length β^{-1}, and attraction strength B in order to see the effects of the competing repulsive and attractive interparticle forces on the system structures. For convenience, we set $m=1$ and $q=1$, so that M and Q are the particle mass and charge, respectively. In addition, we have kept the quadratic confining potential fixed, since our focus here is on the effects of the interparticle repulsive and attractive forces.

III. SIMULATION RESULTS

Before we present our simulation results, let us first look at the effects of the competition between the interparticle repulsive and attractive forces on the potential energy of the interaction. We shall set our parameter range based on Ref. [10], in which particles confined in a 2D trap were found to

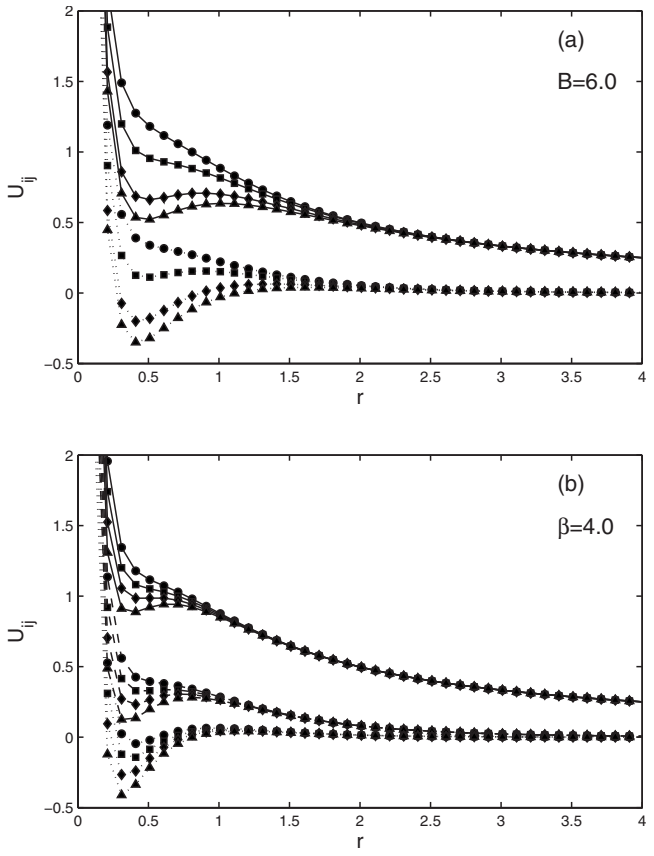

FIG. 1. Interparticle potential energy U_{ij} as a function of the distance r between the particles. (a) The interparticle attraction strength is fixed at $B=6.0$, for inverse repulsive-potential screening lengths $\alpha=0$ (solid lines) and $\alpha=1.1$ (dotted lines), and inverse attractive-potential screening lengths $\beta=2.8$ (triangle), 3.0 (diamond), 3.5 (square), and 4.0 (circle). (b) The inverse attractive-potential screening length is fixed at $\beta=4.0$, for inverse repulsive-potential screening lengths $\alpha=0$ (solid lines), 0.9 (dashed lines), and 1.7 (dotted lines), and attraction strengths $B=6.5$ (circle), 7.0 (square), 7.5 (diamond), and 8.0 (triangle).

self-organize into rings around the trap center when the inverse repulsive-potential screening length $\alpha=0.0$, the inverse attractive-potential screening length $\beta\sim4.0$, and the attraction strength $B\sim6.0$. In this paper, we explore the system configurations in the neighborhood of this regime, i.e., $\beta\leqslant4.0$ at fixed $B=6.0$, and $B>6.0$ at fixed $\beta=4.0$, for different values of α, with the aim of elucidating the effects of the interparticle attractive force on the system steady-state configurations. Figure 1 shows the total interparticle potential energy $U_{ij}(r)$ as a function of the distance r between particles i and j. Note that Fig. 1(a) is for fixed attraction strength $B=6.0$ with different inverse screening lengths of the repulsive (α) and attractive (β) potentials, while Fig. 1(b) is for fixed $\beta=4.0$ with different α and B values. The figures show that at fixed β and B, as the repulsive-potential screening length (α^{-1}) decreases, the potential energy falls rapidly as r increases, so that the particles will encounter a strong interparticle repulsive force at a relatively smaller r. Inclusion of the attractive potential leads to the appearance of a well in the interaction potential, with the minimum at the point where the interparticle attractive and repulsive forces balance. The competition between the interparticle repulsive and attractive forces can be studied by fixing β and α, while adjusting B, or by fixing B and α, while adjusting β, etc. For example, in Fig. 1(b), when α is fixed and $\beta=4.0$, an increase in the attraction strength B decreases the total interparticle potential energy. The increasing dominance of the attractive interparticle force is exhibited by a sharp drop in the potential energy at smaller r, and the appearance of potential minima: at $B=8.0$ when $\alpha=0$; at $B=7.5$ and 8.0 when $\alpha=0.9$; and at $B=6.5-8.0$ when $\alpha=1.7$. When the interparticle repulsive force is reduced by increasing α, the attractive interparticle force exerts greater influence, and one observes an even sharper drop of the total potential energy to a negative value, such as at $B=6.5-8.0$ when $\alpha=1.7$ and $\beta=4.0$. In fact, energy maxima can also be observed in some energy curves, such as that for $\alpha=0$, $\beta=2.8$ and 3.0, and $\alpha=1.1$, $\beta=3.5$ with $B=6.0$ [Fig. 1(a)], and at $\alpha=0$, $B=8.0$ and $\alpha=0.9$, $B=7.5$ and 8.0 with $\beta=4.0$ [Fig. 1(b)], a result of the close competition between the interparticle repulsive and (short-ranged) attractive potentials. Here two configurations are possible: when the particles are close to each other and when they are far from each other. In a confined system, the final system configuration, obtained by minimizing the total system energy, is determined by the combined effects of the interparticle repulsive and attractive forces as well as the external confining force. One expects that the competition between the different forces also leads to structural transitions between the different minimum-energy configurations.

We shall first investigate the minimum-energy configurations of a system consisting of $N=250$ particles at different α and $\beta\leqslant4.0$ for $B=6.0$, and different α and $B>6.0$ at $\beta=4.0$. This should allow us to determine the relative effects of the interparticle attractive and repulsive forces on the system configuration. We shall then consider a larger system with $N=400$ by varying α, β, and B to see if physically new configurations can appear.

A. System with particle number $N=250$

1. Screening effects of the repulsive and attractive forces

Typical minimum-energy configurations of a system with $N=250$ at different inverse repulsive-potential screening length α and inverse attractive-potential screening length β for a fixed attraction strength $B=6.0$ are shown in Fig. 2. The subfigures, all of the same arbitrary scale, are arranged such that the columns show the effects of α, and the rows show the effects of β. A common feature discernible from Fig. 2 is that at a fixed β as α increases, the overall system size is reduced, and the structure becomes more compact. This occurs because an increase in α decreases the strength of the interparticle repulsive force at a fixed interparticle distance, which can also be understood from the potential energy curve shown in Fig. 1(a). Thus the confinement force moves the particles towards the system center, while the attractive interparticle force pulls the particles closer together, resulting in a more compact structure.

The first column of Fig. 2 is for the inverse attractive-potential screening length $\beta=4.0$. One can see configurations

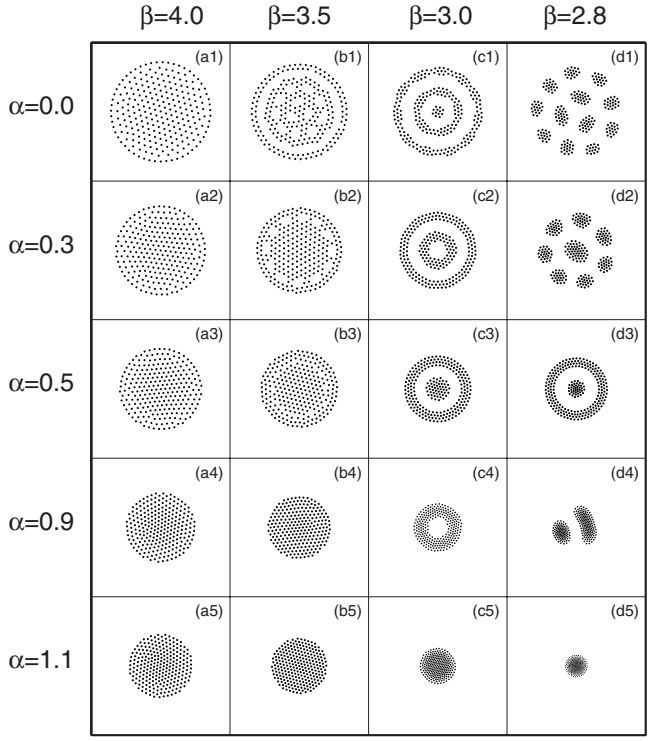

FIG. 2. Calculated minimum-energy configurations of the 2D system at different inverse repulsive-potential screening length α and inverse attractive-potential screening length β with fixed attraction strength $B=6.0$. The total number of particles is $N=250$. The subfigures are of the same arbitrary scale. Note that in (a1), the interparticle repulsion has no screening ($\alpha=0.0$) but the interparticle attraction has strong screening ($\beta=4.0$). In (d1), the repulsion has no screening and the attraction also has a weak screening ($\beta=2.8$), the strong competition between the repulsive and attractive forces causes the particles to group into small clusters. In (d5), the repulsion has strong screening ($\alpha=1.1$) but the attraction has weak screening ($\beta=2.8$), and the particles are grouped into a single dense cluster due to the strong interparticle attractive force.

containing particles arranged in the form of a crystal with a circular outer boundary. These configurations result from the action of the confining central force, which tends to pack the particles into an isotropic configuration. In addition, when $\alpha=0.5$, 0.9, and 1.1 [Figs. 2(a3)–2(a5)], it can be observed that the configurations have become more compact at the system center. This is due to the weakening of the interparticle repulsive force, thus enabling the attractive force to squeeze the particles closer together and the appearance of a denser structure at the system center. Nonetheless, the interparticle repulsive force is still the dominating factor in determining the overall system configuration, since there is no minimum in the interparticle potential energy [Fig. 1(a) when $\beta=4.0$ for $\alpha=0.0$ and 1.1].

The second column of Fig. 2, which is for inverse attractive-potential screening length $\beta=3.5$, shows the occurrence of complex structures at different α values. For example, an outer shell and an inner spongelike structure appear in Fig. 2(b1). The spongelike structure is made up of a cluster of bubbles or voids, i.e., particle-free regions. It is of interest to note that almost everywhere the particles seem to be paired, although the physical significance of this phenomenon is at present unclear. Figure 2(b2) (for $\alpha=0.3$) shows a structure with an inner core which appears as a fairly homogeneous crystal. It is connected to an outer shell by 12 dust-grain bridges. One may surmise that this crystal core is formed by the collapse of the spongy inner core in Fig. 2(b1) because of the reduced repulsive interparticle force. That is, in a system with attractive interparticle force [29], the interparticle repulsive force seems to be necessary for the formation of voids [46–48]. With reduction of the repulsive force, the outer shell now approaches the inner core and the bridges connecting them begin to collapse [see Fig. 2(b3) for $\alpha=0.5$]. A further decrease in the repulsive force produces the expected homogeneous high-density cluster, as can be seen in Figs. 2(b4) and 2(b5) for $\alpha=0.9$ and $\alpha=1.1$, respectively. These results are due to the gradual dominance of the interparticle attractive force [see Fig. 1(a) for $\beta=3.5$]. The decrease in the total interparticle potential energy with the eventual formation of a shallow energy minimum as α increases leads to the transition from the spongelike structures [Figs. 2(b1)–2(b3)] to the high-density clusters [Figs. 2(b4)–2(b5)]. The results here can be relevant to some biological and botanical patterns and can thus be useful in the search for what might be the driving forces behind the latter's formation.

In the third column of Fig. 2, which is for the inverse attractive-potential screening length $\beta=3.0$, one finds patterns of circular shells separated by bandlike voids, with or without a central cluster. Figure 2(c1) shows two shells and a central cluster, but without any bridge. Note that the thickness of the shells is larger than that of Fig. 2(b1) with $\beta=3.5$. This is because a smaller β is associated with an increase in the range of the interparticle attractive force, so that more particles are being drawn to each other, giving rise to a thicker shell. The shells are also observed to be nonuniform in thickness and roughly equally spaced, which is a direct manifestation of the short-ranged nature of the interparticle attractive force. In addition, the interparticle repulsive force ensures a clear separation of the shells from each other. In Fig. 2(c2) for $\alpha=0.3$, one observes a smaller system with two dense shells separated by a bandlike void and a circular central void region. By comparing with Fig. 2(c1), we can infer that the particles in the central cluster for $\alpha=0.0$ have moved outward as α is increased to 0.3. As discussed by Nelissen *et al.* [10], such rearrangement minimizes the overall system energy when the interparticle attraction increases. As α is further increased to 0.5, a dense shell and a central cluster separated by a bandlike void is attained, as shown in Fig. 2(c3). In other words, because of reduced interparticle repulsion the inner shell in Fig. 2(c2) has now collapsed into a cluster. When $\alpha=0.9$, a shell and a central void can be observed, as shown in Fig. 2(c4). When α is further increased to 1.1, the entire system collapses into a small dense cluster, as shown in Fig. 2(c5). The different combinations of concentric shells and bandlike voids are the result of a balance among the competing interparticle forces and the external confinement force in the minimum-energy states. In fact, when $\beta=3.0$, the interparticle potential energy shows a well-defined minimum with a sharper drop in potential energy at small r [see Fig. 1(a)]. This enables the particles to get closer

together to form structures that are more compact. However, at $\alpha=0$ and $\beta=3.0$ with $B=6.0$, an energy maximum also appears in the energy curve, and the combined effects of the interparticle repulsive and attractive forces as well as the confinement force lead to shells with bandlike voids, as shown in Fig. 2(c1). When there is only an energy minimum but not an energy maximum, such as that for $\alpha=1.1$ and $\beta=3.0$ with $B=6.0$ [in Fig. 1(a)], the strong interparticle attractive force draws the particles close together, leading to a single dense cluster as shown in Fig. 2(c5).

When the inverse attractive-potential screening length β drops to 2.8, the last column of Fig. 2 shows that clusters as well as shells appear. In Fig. 2(d1), the particles group into a set of clusters with a fairly regular overall structure when $\alpha=0.0$. Note that the number of particles in each cluster is different. Interestingly, the enhancement in range of the attractive interparticle force has broken up the bands in Fig. 2(c1) (when $\beta=3.0$) to form localized clusters. Such a uniform arrangement of clusters within a 2D trap through a balance among the competing interparticle forces was also discussed in [10,47]. As we switch on the screened potential, the overall system size reduces and seven clusters surrounding a larger cluster at the system center appear [see Fig. 2(d2) for $\alpha=0.3$]. Then, as we adjust the screened potential, a rather radical transformation occurs—the separated clusters at the system edge of Fig. 2(d2) become connected to form a circular shell, resulting in a dense shell surrounding a central cluster [see Fig. 2(d3) for $\alpha=0.5$]. Remarkably, when we further change α to 0.9, the structure of Fig. 2(d3) breaks into two asymmetrically located clusters. Finally, when $\alpha=1.1$, the entire system collapses into a dense cluster [see Fig. 2(d5)]. When $\beta=2.8$ and $\alpha=0$ with $B=6.0$, the interparticle potential energy shown in Fig. 1(a) has an energy minimum as well as an energy maximum. The particles have the tendency to stay closer to each other, but the competition between the interparticle repulsive and attractive forces as well as the confinement force causes the formation of a regular array of clusters, as shown in Fig. 2(d1). When $\beta=2.8$ and $\alpha=1.1$ with $B=6.0$ [in Fig. 1(a)], there is only a deep potential well (energy minimum) without any energy maximum. The strong interparticle attractive force draws the particles together, forming a single dense cluster, as shown in Fig. 2(d5). In the confinement potential, the dense clusters can also be in the form of a single dense shell with a central cluster of particles, as shown in Fig. 2(d3) at $\beta=2.8$ and $\alpha=0.5$ with $B=6.0$.

One can also appreciate the effects of the interparticle attractive force on the minimum-energy configurations by fixing the inverse repulsive-potential screening length α. For example, by examining the first row of Fig. 2 when $\alpha=0.0$ and β is reducing, the particles are observed to change from a uniform crystal-like structure to a configuration with an outer shell and an inner spongelike feature, followed by a structure with two shells and a central cluster separated by bandlike voids, and finally, a regular arrangement of clusters. These transformations show the re-organizing effect determined by the range of the interparticle attractive force. Figure 1(a) for $\alpha=0.0$ shows that as β decreases, the total interparticle potential energy is reduced at small r, showing the increasing influence of the interparticle attractive force.

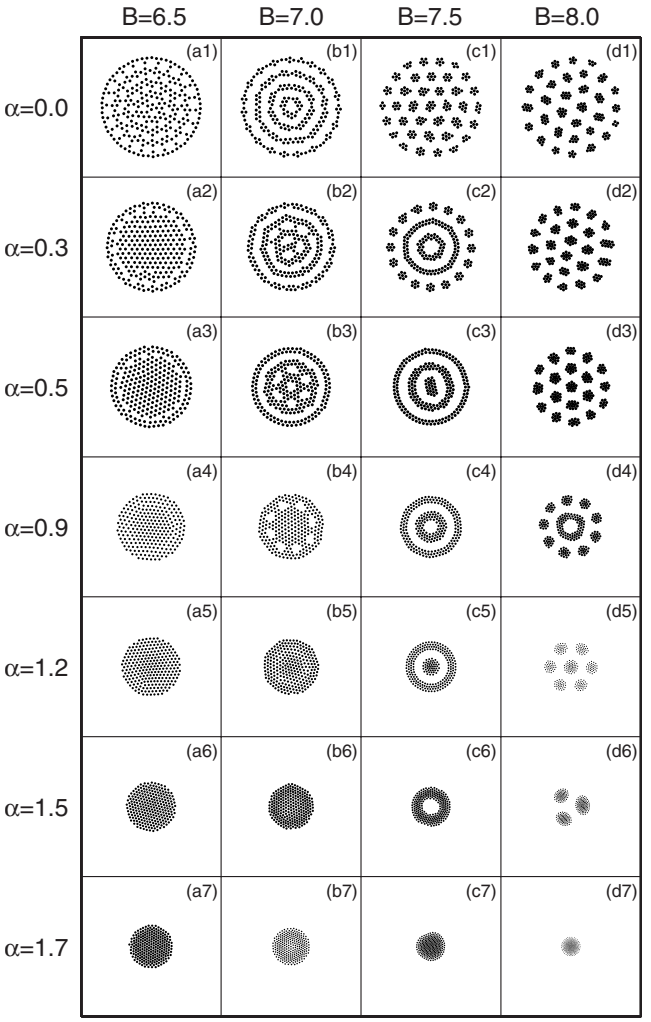

FIG. 3. Calculated minimum-energy configurations at different inverse repulsive-potential screening length α and attraction strength B with a fixed inverse attractive-potential screening length $\beta=4.0$. The total number of particles is $N=250$. The subfigures are of the same arbitrary scale. Note that in the upper left corner (a1), the interparticle repulsion has no screening ($\alpha=0.0$) but the attraction has a strong screening ($\beta=4.0$), however, the relatively strong attraction strength $B=6.5$ leads to a spongelike structure when competing with the interparticle repulsive force. At the upper right corner (d1), the repulsion has no screening (the attraction has a strong screening $\beta=4.0$), but the large attraction strength $B=8.0$ makes the particles grouped into some small clusters, demonstrating the strong interaction competition. At the right bottom corner (d7), the repulsion and attraction both have strong screenings with $\alpha=1.7$ and $\beta=4.0$, respectively, and the large attraction strength $B=8.0$ leads to the formation of a single dense cluster of particles.

2. The effects of inverse repulsive-potential screening length α and attraction strength B

The effects of the competition among the interparticle forces on the system minimum-energy configuration can also be examined from another perspective, which is that it varies inverse repulsive-potential screening length α and attraction strength B (>6.0) while fixing the inverse attractive-potential screening length $\beta=4.0$. Figure 3 shows typical

minimum-energy configurations of a system with $N=250$ for such variations. Note that the columns show the effects of α for a fixed B, while the rows show the effects of B for a fixed α. As before, at a fixed B and β, with increasing α, we expect an overall reduction in the system size, corresponding to the decrease in the interparticle potential energy shown in Fig. 1(b).

By enhancing the interparticle attractive force through increasing attraction strength B from 6.0 to 6.5 at inverse repulsive-potential screening length $\alpha=0.0$ and inverse attractive-potential screening length $\beta=4.0$, a complex structure emerges from the crystal-like structure [see Fig. 3(a1), and compare this structure with that of Fig. 2(a1)]. Interestingly, this new structure has the appearance of a set of shells with bridges of particles connecting between them. At $B=6.5$, as α is increased from 0.0 to 0.3 and 0.5, the system configurations take the form of a shell of particles surrounding a central cluster, with tiny bridges connecting them at random points [see Figs. 3(a2) and 3(a3)]. Furthermore, the particle density at the system center is higher than that at the system edges. When $\alpha \geqslant 0.9$, the entire system has collapsed into a compact cluster due to the weakened interparticle repulsion [see Figs. 3(a4)–3(a7)]. Figures 1(a) and 1(b) show that increasing B from 6.0 to 6.5 at $\alpha=0.0$ and $\beta=4.0$ decreases the interparticle potential energy. However, no energy minimum is observed, implying that the interparticle attractive force is still not strong enough to dominate the total interparticle potential energy to make any abrupt structural changes to the system configuration. Hence the complex configuration remains. However, at $\beta=4.0$ and $B=6.5$, an increase in α leads to a drop in the interparticle potential energy. At $\alpha=1.7$, an energy minimum appears [see Fig. 1(b)], leading to a single dense cluster, as shown in Fig. 3(a7).

Next, we consider a higher attractive interparticle force, namely attraction strength $B=7.0$. As shown in Fig. 3(b1), four thin and equally spaced shells with nonuniform thickness are observed. By comparing with the configuration shown in Fig. 3(a1), we observe that the intershell bridges have been destroyed by a greater short-ranged attractive force. When $\alpha=0.3$, a complex structure, with an outer shell and two connected noncircular inner shells with a central cluster, is formed [see Fig. 3(b2)]. When α becomes 0.5, three shells appear with six bridges linking the inner two shells, resulting in a structure with six small voids and a central void [Fig. 3(b3)]. These seven voids are organized into a hexagonal configuration by a delicate balance among the forces acting on the particles. At $\alpha=0.9$, the connected inner shells of Fig. 3(b3) have collapsed into a compact cluster, which then joins with the outer shell through eight bridges. The resulting structure is a regular array of eight small voids [see Fig. 3(b4)]. For $\alpha \geqslant 1.2$, Figs. 3(b5)–3(b7) show that the entire system has collapsed into a dense cluster. Figure 1(b) shows that at fixed $\beta=4.0$ and $\alpha=0.0$, as B increases from 6.5 to 7.0, the interparticle potential energy decreases without the appearance of an energy minimum. The strong competition among the interparticle forces leads to the formation of several thin shells separated by bandlike voids. On the other hand, when $\beta=4.0$ and $B=7.0$, an energy minimum starts to appear in the potential energy when $\alpha=1.7$ [Fig. 1(b)], demonstrating the dominance of the interparticle attractive force. The result is a single dense cluster as shown in Fig. 3(b7).

Let us now set attraction strength B to 7.5 and examine the minimum-energy states at different α values. Under the action of a pure Coulomb repulsive interparticle force ($\alpha=0.0$), many small clusters arranged in a crystal-like structure appear [see Fig. 3(c1)]. As discussed in Ref. [10], each cluster can be treated as a particle with effective mass and charge. Compared to Fig. 3(b1), one observes that the shells have broken up into small clusters due to a new balance of forces triggered by an increase in the interparticle attractive force. Increasing α to 0.3, the inner clusters become connected, forming two closed shells as the attractive force draws the particles together as the repulsive force weakens. However, the repulsive force is still strong enough to prevent the joining up of the clusters at the system edge. Hence small clusters remain at the outer ring which surrounds the two inner shells [see Fig. 3(c2)]. A further weakening of the repulsive force with $\alpha=0.5$ then enables the attractive force to connect up these clusters to form a closed shell, while the innermost shell of Fig. 3(c2) collapses into a central cluster [see Fig. 3(c3)]. By increasing α to 0.9, 1.2, 1.5, and 1.7, the minimum-energy configurations are found to possess the respective forms of Figs. 2(c2)–2(c5) [see Figs. 3(c4)–3(c7)]. Based on the interparticle potential energy given in Fig. 1(b), one can see that complex particle configurations occur before the appearance of clear energy minima in the interparticle potential energy when $\beta=4.0$ and $B=7.5$. When $\alpha=0.9$, there is a minimum as well as a maximum in the potential energy, and the delicate competition between the interparticle repulsive and attractive forces as well as the confinement force leads to the formation of shells separated by a bandlike void, as shown in Fig. 3(c4). At $\alpha=1.7$ and $B=7.5$ with $\beta=4.0$, there is only a minimum in the potential energy, and the strong attractive force draws the particles together, forming a single dense cluster, as shown in Fig. 3(c7).

Finally, we set the attraction strength B to 8.0. With a larger interparticle attractive force, the particles have a greater tendency to gather into clusters and organize into crystal-like structures [see Figs. 3(d1)–3(d3)]. The clusters are also denser and more separated from each other. As the interparticle repulsive force is reduced, the clusters begin to approach each other. At $\alpha=0.9$, the inner clusters become close enough for the attractive force to dominate. A closed shell surrounded by an outer ring of clusters is formed, as shown in Fig. 3(d4). When $\alpha=1.2$, the system of particles gets even closer together, leading to the formation of seven clusters, which are organized into a hexagonal structure [see Fig. 3(d5)]. Then, at $\alpha=1.5$, three clusters appear [see Fig. 3(d6)]; and the entire system collapses into a single small dense cluster as α reaches 1.7 [see Fig. 3(d7)]. These transitions can be understood from Fig. 1(b) when $\beta=4.0$ and $B=8.0$. For example, at $\alpha=0.0$ and 0.9, both minimum and maximum appear in the interparticle potential energy, leading to the formation of small clusters, as shown in Figs. 3(d1) and 3(d4). At $\alpha=1.7$ and $B=8.0$, with only an energy minimum in the potential energy [in Fig. 1(b)], the strong attractive force leads to a single dense cluster, as shown in Fig. 3(d7).

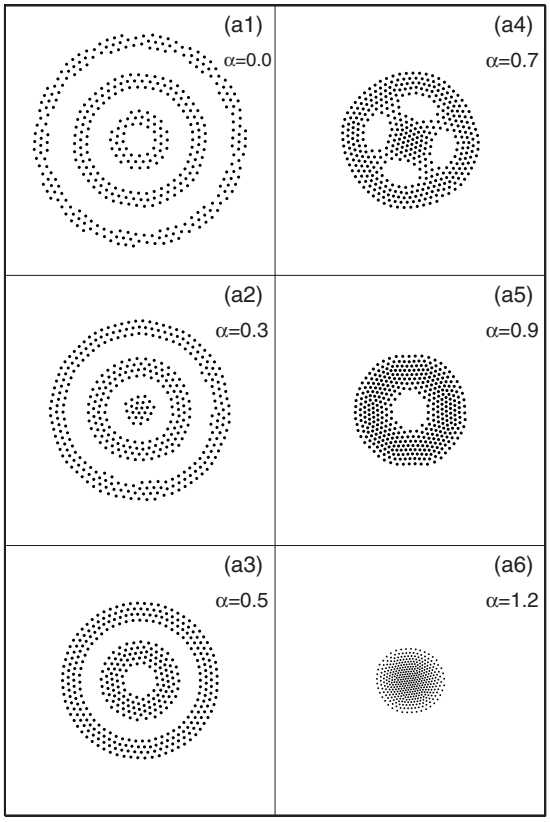

FIG. 4. Calculated minimum-energy configurations at different inverse repulsive-potential screening length α for the inverse attractive-potential screening length $\beta=3.0$ and attraction strength $B=6.0$. The total number of particles is $N=400$. The subfigures are of the same arbitrary scale. Competition between the interparticle repulsion and attraction leads to the different system configurations at different levels of the inverse repulsive-potential screening length α.

These results show that different system configurations can be obtained through varying the parameters β, B, and α. In particular, when $\beta=3.0$ and $B=6.0$ [refer to Figs. 2(c1)–2(c5)] or $\beta=4.0$ and $B=7.5$ [see Figs. 3(c3)–3(c7)], concentric shells separated by bandlike voids are observed, which is due to the delicate balance among the interparticle repulsive and attractive forces as well as confinement force acting on the particles in minimizing the total system energy. When there are minimum and maximum observed in the interparticle potential energy, the configurations such as shells separated by bandlike voids and the clusters organized in a crystal-like structure are likely to be formed. In fact, similar structures of shells separated by bandlike voids have been detected in a dusty plasma system [23–25].

B. System with particle number $N=400$

1. The effect of inverse attractive-potential screening length $\beta=3.0$ and attraction strength $B=6.0$

Figure 4 shows the typical minimum-energy configurations of a system with $N=400$ particles at the inverse attractive-potential screening length $\beta=3.0$ and attraction strength $B=6.0$, for different values of the inverse repulsive-potential screening length α. As the range of parameters employed in Fig. 4 almost corresponds to those of Figs. 2(c1)–2(c5), we expect the corresponding system configurations to be similar. This is indeed the case except the structure in Fig. 4(a4). In Fig. 4(a1) for $\alpha=0.0$, one finds three concentric shells, two bandlike voids, and a central void. As α is increased to 0.3, the overall size of the system falls, with the innermost shell collapses into a central cluster because of the reduced interparticle repulsion [see Fig. 4(a2)]. One sees that a larger particle number leads to thicker shells, which increases the possibility of bridging between the shells. This occurs at $\alpha=0.7$ [see Fig. 4(a4)], where four bridges connect an inner cluster to the outer shell, leading to four voids organized into a regular structure. Thus for a system consisting of a larger number of particles, not only concentric shells separated by bandlike voids, but also multivoids, can occur. In dusty plasma system, as discussed in Refs. [23–25], such multivoid configurations have yet to be observed.

2. Inverse attractive-potential screening length $\beta=4.0$ and attraction strength $B=7.5$

The effect of particle number is easily discernible in this parameter range when compared with the corresponding configurations shown in Figs. 3(c1)–3(c7). In Fig. 5(a1) when inverse repulsive-potential screening length $\alpha=0.0$, instead of small clusters arranged in a crystal-like structure, the minimum-energy configuration now takes the form of two closed inner shells surrounded by shells that are broken by clusters of particles. More precisely, the outermost shell is almost completely broken into small clusters, but the neighboring shell is only partially broken. The particles are organized into different lines on a ring or a shell. Similar broken-shell stripes were also reported in Ref. [10]. As α is increased to 0.3 and 0.5, configurations with closed shells and bandlike voids are formed, as shown in Figs. 5(a2) and 5(a3). Noting again that larger particle number tends to form thicker shells, one expects bridgelike structures to appear. This indeed happens at $\alpha=0.9$, for which the system size is greatly reduced and the density has become higher. Bridges appear between the shells and the central cluster, resulting in 11 small voids. The voids are organized into a regular structure, with three voids located near the system center and eight voids surrounding them, as shown in Fig. 5(a4). A further increase of α to 1.1 leads to the appearance of two shells that are bridged together. The seven voids between the bridges form a hexagonal structure, as shown in Fig. 5(a5). At $\alpha=1.2$ the entire system becomes more compact, with one shell bridged to a central cluster, with five voids arranged into a pentagon structure, as shown in Fig. 5(a6). Finally, increasing α to 1.5 and 1.8 leads to structures that are similar to that of Figs. 3(c6) and 3(c7), respectively [see Figs. 5(a7) and 5(a8)].

We have also considered the $N=400$ system for other values of β, B, and α as in Figs. 2 and 3. It is found that the configurations obtained at different α values exhibit similar features as that in Figs. 2 and 3 for the same values of β and B, except that the entire system is larger in size. Only the results for $\beta=3.0$, $B=6.0$ and $\beta=4.0$, $B=7.5$ are displayed

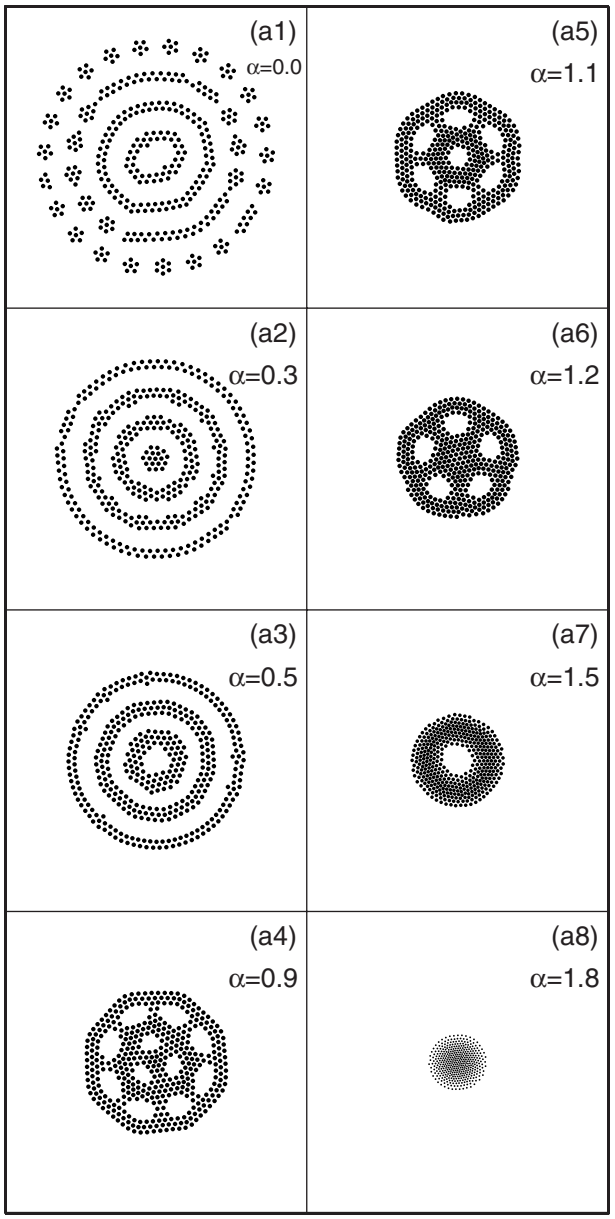

FIG. 5. Calculated minimum-energy configurations at different inverse repulsive-potential screening length α for the inverse attractive-potential screening length $\beta=4.0$ and attraction strength $B=7.5$. The total number of particles is $N=400$. The subfigures are of the same arbitrary scale. Competition between interparticle repulsion and attraction leads to a wide variety of system configurations at different levels of the inverse repulsive-potential screening length α.

since they possess more distinct features, such as the regular multiple voids. These structures are a consequence of the complex competition among the different forces acting on the particles in the minimum-energy states.

IV. CONCLUSIONS

We have investigated the self-assembly of a 2D system of single-species of charged particles in a quadratic trap, interacting through a pure or screened Coulomb repulsive potential and a short-ranged attractive potential by means of MD simulation. Our results show that a wide variety of minimum-energy configurations can occur as we vary the strengths of the interparticle repulsive and attractive forces. More specifically, at the inverse attractive-potential screening length $\beta=3.0$ and attraction strength $B=6.0$, or $\beta=4.0$ and $B=7.5$, we found that concentric shells separated by bandlike voids, and connected shells with regular patterns of multivoids, such as hexagonal and pentagonal patterns, can be obtained at suitable levels of the screened repulsive interparticle potential. These system configurations are due to the complex competition among the interparticle repulsive and attractive forces as well as the confinement force acting on the particles in minimizing the total system energy. When there are minimum and maximum observed in the interparticle potential energy, configurations such as shells separated by bandlike voids and the clusters organized in a crystal-like structure are likely to be formed. Furthermore, when the number of particles in the system becomes large, we found that an even larger range of patterns becomes feasible. It is interesting that the intricate balance between the interparticle repulsive and attractive forces, together with the confinement force, can give rise to such a variety of complex patterns.

In earlier studies on 2D dusty plasma systems consisting of multispecies charged particles with equal mass-to-charge ratio confined in a quadratic trap, it was found that system configurations with concentric shells separated by bandlike voids can only be obtained if the systems are also subjected to a radially outward drag force [23–25]. In a single-species system under a strong drag force, the only possible configuration is a single shell with a central void [23–26]. Theoretical studies have also found that the ion drag force is necessary for void formation in dusty plasmas [27,28]. In Liu *et al.*'s studies [23–25], the attractive interparticle force [26,34,49] was introduced to simulate the cohesive effects of the background plasma and neutral particles on the charged dusts in the experiments, and the strength of the attractive force is very weak in comparison with the interparticle repulsive force in affecting the system configurations. According to our results, if the interparticle attractive force is strong enough, even in absence of the ion drag force, the concentric shells with bandlike voids can occur in a single-species particle system confined by a quadratic trap. However, in dusty plasmas, it is unclear how strong is the attractive interparticle force, and how are the particle charge and mass distributed in the experiments [25]. The dust grains in these dusty plasma experiments were chemically synthesized, and the structures of concentric shells and bandlike voids are only observed during the evolution of the grain growth process. A detailed comparison between simulation and experimental results is only possible if the charge and mass distributions of these dust grains can be measured. On the other hand, in colloidal polymer dispersions voids have also been observed in the absence of any outward drag force [29]. This implies that there must exist an attractive force between the colloidal particles, as researchers have already suggested [21,22,29].

Although our results are for 2D systems, they can be useful in roughly predicting pattern formations in a corresponding three-dimensional (3D) systems, since the force balance in a 2D cross section of a 3D system can be similar to the 2D

system. In 3D systems, structures such as concentric spherical shells separated by spherical-shell voids, spherical shells with a uniform arrangement of multivoids, and spherical shell with solid clusters, have also been observed in polymer surfactant nanodroplets systems [50], amphiphilic block copolymer solutions [51], as well as charged dust systems [25]. The studies here can provide a perspective on the manner in which charged particles self-organize under competing forces. Our results on pattern structures can also be useful in the design and creation of specific micro- and nanoscale functional materials for modern technological applications such as microfuel cells, high-capacity batteries, efficient catalysts and sensors [30]. Appropriate patterning of semiconductor and other materials is also crucial in modern microelectronics and optoelectronics, as well as in tissue engineering, drug delivery, microfluidics, etc. Our results can also serve as a guide for future experiments and theories on the effects of interparticle forces in complex systems such as the dusty plasmas and the colloidal solutions.

ACKNOWLEDGMENTS

The authors thank Z. Y. Chen for useful discussions. This work was partially supported by the NNSFC (Project No. 10835003).

[1] M. Engel and H. R. Trebin, Phys. Rev. Lett. **98**, 225505 (2007).
[2] G. M. Whitesides and B. Grzybowski, Science **295**, 2418 (2002).
[3] O. D. Velev, Science **312**, 376 (2006).
[4] A. I. Campbell, V. J. Anderson, J. S. van Duijneveldt, and P. Bartlett, Phys. Rev. Lett. **94**, 208301 (2005).
[5] P. J. Lu, J. C. Conrad, H. M. Wyss, A. B. Schofield, and D. A. Weitz, Phys. Rev. Lett. **96**, 028306 (2006).
[6] C. Kittel, Phys. Rev. **70**, 965 (1946).
[7] B. A. Grzybowski, J. A. Wiles, and G. M. Whitesides, Phys. Rev. Lett. **90**, 083903 (2003).
[8] C. Reichhardt, C. J. Olson Reichhardt, I. Martin, and A. R. Bishop, Phys. Rev. Lett. **90**, 026401 (2003).
[9] C. J. Olson Reichhardt, C. Reichhardt, and A. R. Bishop, Phys. Rev. Lett. **92**, 016801 (2004).
[10] K. Nelissen, B. Partoens, and F. M. Peeters, Phys. Rev. E **71**, 066204 (2005).
[11] B. Liu and J. Goree, Phys. Rev. E **75**, 016405 (2007).
[12] S. W. S. Apolinario, B. Partoens, and F. M. Peeters, Phys. Rev. E **74**, 031107 (2006).
[13] S. A. Khrapak, S. K. Zhdanov, A. V. Ivlev, and G. E. Morfill, J. Appl. Phys. **101**, 033307 (2007).
[14] B. Liu and J. Goree, Phys. Rev. Lett. **100**, 055003 (2008).
[15] M. E. Leunissen, C. G. Christova, A. P. Hynninen, C. P. Royall, A. I. Campbell, A. Lmhof, M. Dijkstra, R. van Roij, and A. van Blaaderen, Nature (London) **437**, 235 (2005).
[16] K. Nelissen, B. Partoens, and F. M. Peeters, Europhys. Lett. **79**, 66001 (2007).
[17] S. A. Khrapak, B. A. Klumov, and G. E. Morfill, Phys. Rev. Lett. **100**, 225003 (2008).
[18] S. A. Khrapak, G. E. Morfill, V. E. Fortov, L. G. D'yachkov, A. G. Khrapak, and O. F. Petrov, Phys. Rev. Lett. **99**, 055003 (2007).
[19] G. L. Delzanno, G. Lapenta, and M. Rosenberg, Phys. Rev. Lett. **92**, 035002 (2004).
[20] F. Sciortino, Nature Mater. **1**, 145 (2002).
[21] T. Eckert and E. Bartsch, Phys. Rev. Lett. **89**, 125701 (2002).
[22] K. N. Pham, A. M. Puertas, J. Bergenholtz, S. U. Egelhaaf, A. Moussaïd, P. N. Pusey, A. B. Schofield, M. E. Cates, M. Fuchs, and W. C. K. Poon, Science **296**, 104 (2002).
[23] Y. H. Liu, Z. Y. Chen, F. Huang, M. Y. Yu, L. Wang, and A. Bogaerts, Phys. Plasmas **13**, 052110 (2006).
[24] Y. H. Liu, Z. Y. Chen, M. Y. Yu, and A. Bogaerts, Phys. Rev. E **74**, 056401 (2006).
[25] F. Huang, M. F. Ye, L. Wang, and N. Jiang, Chin. Phys. Lett. **21**, 121 (2004).
[26] R. P. Dahiya, G. V. Paeva, W. W. Stoffels, E. Stoffels, G. M. W. Kroesen, K. Avinash, and A. Bhattacharjee, Phys. Rev. Lett. **89**, 125001 (2002).
[27] M. Kretschmer, S. A. Khrapak, S. K. Zhdanov, H. M. Thomas, G. E. Morfill, V. E. Fortov, A. M. Lipaev, V. I. Molotkov, A. I. Ivanov, and M. V. Turin, Phys. Rev. E **71**, 056401 (2005).
[28] A. M. Lipaev, S. A. Khrapak, V. I. Molotkov, G. E. Morfill, V. E. Fortov, A. V. Ivlev, H. M. Thomas, A. G. Khrapak, V. N. Naumkin, A. I. Ivanov, S. E. Tretschev, and G. I. Padalka, Phys. Rev. Lett. **98**, 265006 (2007).
[29] K. Ito, H. Yoshida, and N. Ise, Science **263**, 66 (1994).
[30] K. Ostrikov, Rev. Mod. Phys. **77**, 489 (2005).
[31] D. Samsonov and J. Goree, Phys. Rev. E **59**, 1047 (1999).
[32] G. E. Morfill, H. M. Thomas, U. Konopka, H. Rothermel, M. Zuzic, A. Ivlev, and J. Goree, Phys. Rev. Lett. **83**, 1598 (1999).
[33] J. Goree, G. E. Morfill, V. N. Tsytovich, and S. V. Vladimirov, Phys. Rev. E **59**, 7055 (1999).
[34] V. N. Tsytovich, S. V. Vladimirov, G. E. Morfill, and J. Goree, Phys. Rev. E **63**, 056609 (2001).
[35] K. Nelissen, A. Matulis, B. Partoens, M. Kong, and F. M. Peeters, Phys. Rev. E **73**, 016607 (2006).
[36] Y. H. Liu, B. Liu, Y. P. Chen, S. Z. Yang, L. Wang, and X. G. Wang, Phys. Rev. E **67**, 066408 (2003).
[37] J. H. Chu and L. I, Phys. Rev. Lett. **72**, 4009 (1994).
[38] V. M. Bedanov and F. M. Peeters, Phys. Rev. B **49**, 2667 (1994).
[39] V. A. Schweigert and F. M. Peeters, Phys. Rev. B **51**, 7700 (1995).
[40] J. A. Drocco, C. J. Olson Reichhardt, C. Reichhardt, and B. Jankó, Phys. Rev. E **68**, 060401(R) (2003).
[41] Y. H. Liu and L. Y. Chew, J. Phys. A **40**, 10383 (2007).
[42] W. P. Ferreira, J. C. N. Carvalho, P. W. S. Oliveira, G. A. Farias, and F. M. Peeters, Phys. Rev. B **77**, 014112 (2008).
[43] Y. H. Liu and L. Y. Chew, J. Phys.: Condens. Matter **19**, 356213 (2007).
[44] W. G. Hoover, Phys. Rev. A **31**, 1695 (1985).

[45] L. Verlet, Phys. Rev. **159**, 98 (1967).
[46] Y. J. Lai and L. I., Phys. Rev. E **60**, 4743 (1999).
[47] I. Denysenko, M. Y. Yu, L. Stenflo, and N. A. Azarenkov, Phys. Plasmas **12**, 042102 (2005).
[48] K. Avinash, A. Bhattacharjee, and S. Hu, Phys. Rev. Lett. **90**, 075001 (2003).
[49] Y. P. Chen, H. Luo, M. F. Ye, and M. Y. Yu, Phys. Plasmas **6**, 699 (1999).
[50] J. G. E. M. Fraaije and G. J. A. Sevink, Macromolecules **36**, 7891 (2003).
[51] X. He and F. Schmid, Phys. Rev. Lett. **100**, 137802 (2008).